Design and Development of Filter Wheel Controller Card, Temperature Controller and Automated Software using Labview for CMAP Instrument

by

Pankaj K. Kushwaha, Shashank Urmalia, Duggirala Pallamraju, Ravindra P. Singh & Pradip Suryawanshi
(Space & Atmospheric Sciences Division)

भौतिक अनुसंधान प्रयोगशाला, अहमदाबाद
Physical Research Laboratory, Ahmedabad

https://www.prl.res.in/

Design and Development of Filter Wheel Controller Card, Temperature Controller and Automated Software using Labview for CMAP Instrument

Pankaj K. Kushwaha[*], Shashank Urmalia, Duggirala Pallamraju, Ravindra P. Singh & Pradip Suryawanshi

Abstract

In this report we present technical details of the design and development of filter wheel and bipolar temperature controller cards that are required for controlling the position and temperature of the optical filters in the in-house built CCD-based multiwavelength Airglow Photometer (CMAP). In order to control the various functions of the CMAP, a Labview based fully automated software has been developed which acquires data in the desired format and controls various modules of CMAP in a synchronized manner. This software continuously monitors various parameters and facilitates the smooth operation of CMAP in an automated mode. This report provides the design details along with the schematic and PCBs of the stepper based filter wheel controller and bipolar temperature controller cards. Further, we also present the details of the development of the software using LabView for controlling the operations of CMAP and of storing the CCD images in FITS format. Finally, we demonstrate the field operations of the integrated system which includes all the in-house developed subsystems.

Keywords

Optical Photometers, Airglow, Temperature Controller, Filter wheel, Labview Data Acquisition, CCD Imaging using Labview, stepper motor control using Labview.

Contents

1. Introduction

The Earth's upper atmosphere (UA) is influenced by forcing from above by the solar radiation and from below by the upward propagating atmospheric waves from the lower atmosphere. Therefore, various parameters of the UA e.g., temperature, density, pressure, composition show changes of different time scales in response to these forcings. Hence, in order to gain an understanding of the behavior of the upper atmosphere due to various sources, it is important to characterize their effects at various time scales and at different altitudes. For this purpose, passive remote sensing of naturally occurring airglow emissions at different wavelengths is an effective means. In this report, we describe the development of a multiwavelength nightglow photometer that is capable of near-simultaneous measurement of nightglow emissions that emanate from five different altitudes in the Earth's UA.

The atmospheric molecules in the UA get photodissociated during daytime in the presence of solar radiation and some of them remain in the atomic form during nighttime due to low pressure in the UA. There are various chemical reactions that occur in the UA which show a strong response to the incident solar radiation and the densities of the reacting atoms/molecules. As a result, various neutrals, ionized atoms, and molecules get to their excited states. During their de-excitation, photons are emitted that are characteristic of the energy state of emitting species which range from ultraviolet to infrared wavelengths of the electromagnetic spectrum and this is called airglow. Airglow measurements, both during daytime and nighttime, have been used effectively to investigate the neutral behavior of the upper atmosphere. Measurement of airglow emission intensity can be carried out using various optical techniques e.g., photometry, spectroscopy, and interferometry.

For optical aeronomy studies, some of the important emissions exist in the wavelength range of 400 nm to 900 nm. It is not possible to cover the whole spectral range by using a single portable optical instrument required for the optical aeronomy applications. However, as some airglow emissions emanate at a few discrete wavelengths in the visible spectral region, by using various narrowband interference filter (NBIF) whose central transmissions peak lies at the airglow emission wavelengths, it is possible to accommodate this in a single photometer. In order to achieve this, one has to develop a stepper motor based filter wheel to bring different filters in the optical path of this photometer. As the transmission efficiency of these narrow bandwidth interference filters is dependent on temperature, it is required that the temperature of the filter chamber is maintained at a fixed value. Therefore, a temperature controller needs to be developed that controls the temperature of the filters to avoid shifts in the wavelength of peak transmissions of these optical filters which maintain the same temperature of the interference filters within the tolerance limit. Hence, the filter chamber is optimally fixed at the temperatures at which commercial off the shelf (COTS) filters are available.

The first version of CMAP was developed by using a commercially available filter wheel which was augmented with temperature controllers and software had been developed to run it in automated mode (Phadke et al., 2014). In order to understand the vertical coupling processes of the UA it is required to carry out simultaneous measurement of different airglow emission intensities that originates from different altitudes (Laskar et al., 2013). These kinds of studies in the nighttime has been carried out using CMAP observation as it provides nigthglow emission brightness from different altitudes continuously in an unattended mode of operation (Singh and Pallamraju, 2016).

The new requirement is to carry out nightglow observations in near infrared region which was not possible with the earlier version of the CMAP as it uses a CCD that has very low quantum efficiency in the near infrared region. Therefore, in this second version of CMAP, we have replaced the earlier CCD with a new CCD that is sensitive to the near infrared wavelengths. It is also required to operate these instruments from various strategic locations in India. Therefore, it is essential to indigenously develop various hardware, mechanical systems, filter wheel and temperature controller card, and a single GUI based automated software which interfaces with all the subsystems. This has been achieved using Labview based GUI software which integrates all the components of the newly developed CMAP wherein data acquisition has been carried out in a seamless manner. Due to the indigenous development of the different subsystems, the newly developed CMAP has now become more flexible, robust, easy to replicate and maintain, cost effective, and easy for troubleshooting. Thus, it can be operated from remote locations with minimal manual intervention.
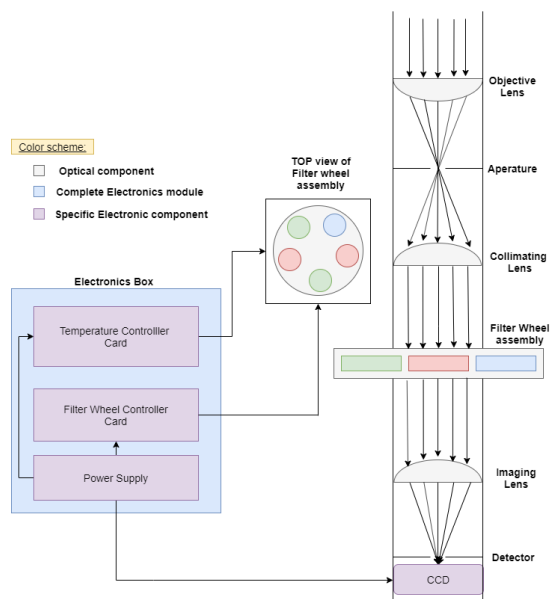

Figure 1. Block diagram of CMAP showing optical layout and electronic modules.

2. Different Subsystem of CCD-based Multiwavelength Airglow Photometer (CMAP)

In this section, the optical layout and design of CMAP will be discussed. Figure 1 shows the schematic diagram of the newly developed CMAP which consist of various optical components (as discussed in Figure 2) required for electronic modules like temperature controller card, filter wheel controller card, power supply, and CCD.
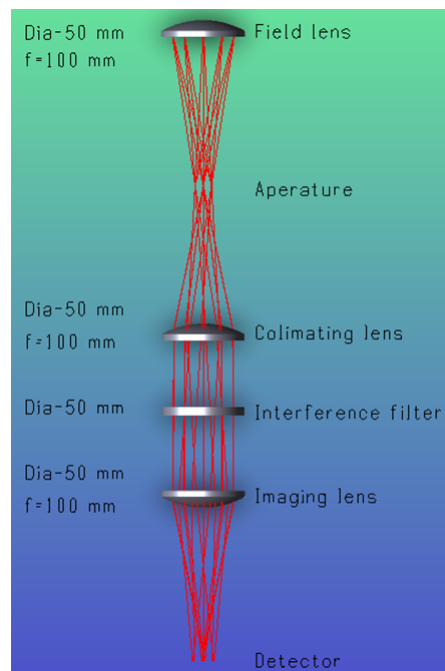
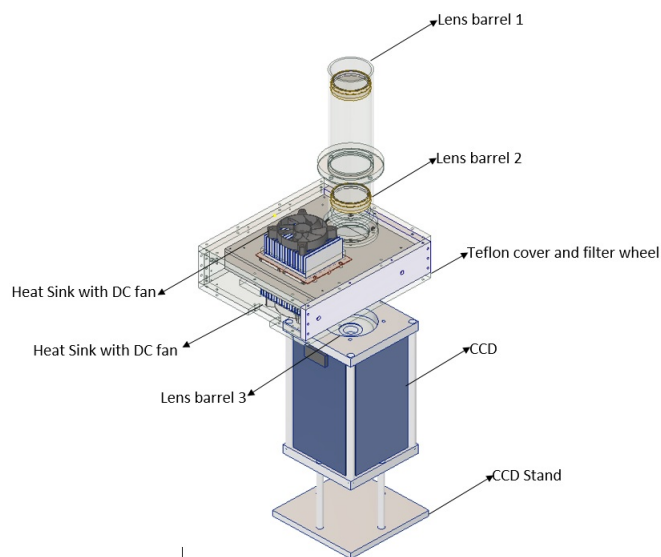

Figure 2. Zemax design of CMAP.

Figure 3. CAD design showing different mechanical subsystems used for the fabrication of CMAP.

Figure 2 shows the Zemax design of CMAP which consist of a field lens to focus the incoming rays on to the aperture, collimating lens is used to make the beam parallel, interference filters are used to pass the desired wavelength on to the imaging lens, and imaging lens focuses the incoming beam on to the detector. The present design of CMAP follows the #f/2 optics.

The Computer-aided design (CAD) of the CMAP is given in Figure 3. We have designed all the mechanical subsystems by using Autodesk Inventor software and have been fabricated in the PRL workshop. Special care has been taken to avoid the light leakage in the CMAP which has been carried out by overlapping one mechanical assembly part on to another at all connecting interfaces. After the assembly, the system is checked for light leakage. All the hardware components are joined via a screw and threaded joints as shown in Figure 3 without affecting the other components. As mentioned earlier, it is required to minimize the effect of ambient temperature fluctuation on the filter assembly. Therefore, the filter wheel assembly is covered with an additional teflon assembly, as it has a very low thermal conductivity and so it serves the purpose of thermal insulation.

2.1 CCD (Charge Coupled Device)

Historically, Photo Multiplier Tubes (PMTs) have been used in airglow photometers (e.g., Narayanan et al., 1989, Pallamraju et al., 1996, Sridharan et al., 1998, Chakrabarty, 2007 and Sarkhel, 2010). Photons striking a photocathode at the entrance window of a PMT produces electrons, which are then accelerated by a high-voltage field and multiplied in numbers by using a chain of dynodes to produce optimal amplification of the signal. In PMT the current generated is directly proportional to the amount of photons incident on the photocathode.

On the other hand, CCD uses semi-conductor chips as

detectors. The detector collects the photon which generates a voltage that corresponds to photons collected. These photons are stored in the capacitors and therefore, unlike PMTs they are not damaged due to over-exposure. In addition, CCD requires less power and have higher quantum efficiency which makes them superior to PMTs. Also, the signal to noise ratio (SNR) of the whole system can improve in the CCD based systems as it is possible to choose only photons falling on a certain region of interest, thereby photon noise scattering in the instrument and readout noise can be reduced. The CCDs come with their software development kit (SDK) using which several parameters can be controlled to enable their operation in programmed mode. To customize the operations, we need to develop our own software through which we can control the CCD parameters, like binning, exposure time, detector chip cooling temperature, the region of interest, etc., while synchronizing it with filter wheel rotation in an automated mode. For indigenous development of instrument it is also required to develop such software for CCD which is compatible with the in-house built electronics of the instrument, such as the filter wheel and temperature controller cards. To cater the requirements as mentioned above, it was decided to use Labview as the interface software. Andor make CCD was used which has good quantum efficiency in the NIR region this is required to cover large spectral range of nightglow emissions. In the present CMAP, we have used a commercial CCD having quantum efficiency (QE) greater than 85% in spectral region of 400 nm - 900 nm as shown in Figure 4 (BEX2-DD model of andor 1K×1K CCD is used). In this work, we have also developed the software to operate and store the data at pre-defined settings of the CMAP using Labview software.
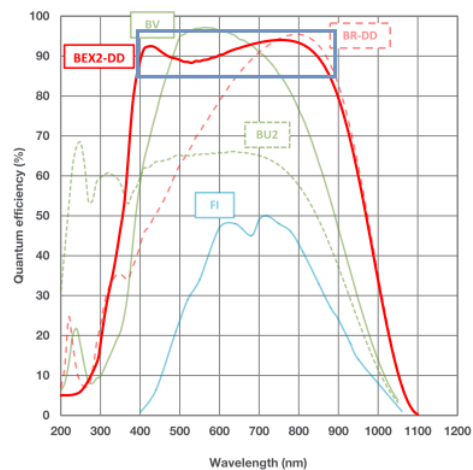

Figure 4. CCD quantum efficiency curve shows QE greater than 85% for 400 nm - 900 nm spectral range for BEX2-DD.
(Courtesy-https://https://andor.oxinst.com)

In summary, the use of CCDs in this photometry technique has revolutionized the thinking and made the CMAP a very versatile, reliable, durable, and easy to be operate in

programmed and automated mode day-after-day in remote locations as well. These are: (i) being a solid state detector, it does not get over-saturated, (ii) CCD uses low-voltages which are more desirable for remote operations as compared to PMT which requires operating voltage of the order of KV, (iii) the quantum efficiency of the CCD covers almost all of the CMAP applications for nighttime aeronomy studies, (iv) being an imaging detector, it gives us a handle on appropriately taking care of the background scattering effect by considering the light falling on the neighbouring pixels than the ones where airglow data falls, which is otherwise not possible. It is true that the PMT has the ability to go for lower read out noise (zero) compared to a CCD, and sensitivity and capability of detecting single photon is also significant. Nevertheless, all the above mentioned factors were considered in deriving the signal-to-noise ratio, and it was found that the CCD is suitable with an integration of 1 minute.

2.2 Filter Wheel

As discussed, in order to study the upper atmospheric emissions originating at different altitudes, we need to cover spectral region ranging from 400 nm to 900 nm, and at the same time it is required that the bandwidth of the interference filters is small in order to increase the SNR of the photons collected. We use multiple NBIF filters of different central wavelengths, that are chosen depending on the scientific interest. The present working model consists of 5 filters as shown in Figure 1. In the current setup we are measuring OI (557.7 nm) and OI (630 nm) emissions that originate from altitude centered at 100 km and 230 km, respectively. To measure mesospheric temperatures we use $P_1(2)$ and $P_1(4)$ rotational lines at 840.0 nm and 846.5 nm wavelengths of OH (6-2) band emissions which originate from 87 km altitude. An additional filter at 857.0 nm measures the background that needs to be subtracted from the nightglow data for unambiguous derivation of temperatures using OH (6-2) band emissions (Singh and Pallamraju, 2017) (Singh, 2017). The optical filters have central wavelengths at: λ_1= 557.7 nm, λ_2 = 630.0 nm, λ_3 = 840.0 nm, λ_4 = 846.6 nm and λ_5 = 857.0 nm and have bandwidths in the range of 0.3 nm to 0.5 nm. The Filter wheel assembly consists of a stepper motor, stepper motor driver (A4988), Arduino Uno board and Hall effect sensor (OH180U) as shown in Figure 5.
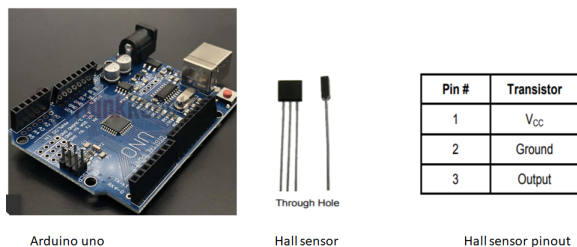

Pin #	Transistor
1	V_{CC}
2	Ground
3	Output

Figure 5. Arduino Uno, Hall sensor and its pinout.

To achieve precise rotation of filter wheel we have used a stepper motor along with an A4988 stepper motor driver. The motor should rotate in such a way that it logs its initial position (filter1 position) using a Hall effect sensor for determining the filter sequence. Profile file settings such as exposure time are used to determine the stop time for each filter position. We have used a five-position filter wheel assembly obtained from spectral products. The total inertial load (due to filter wheel pulley, belt, filters, motor, driving pulley) for the five-position filter wheel is 1.07 Kg-cm^2. As per our calculations, a torque of 1.95×10^{-2} Kg-cm @ 90 rpm is suitable for the required operation. The maximum holding torque of the spectral product motor used in the filter wheel is well above this value. Hence, we have used the filter wheel hardware from spectral products. However, for our customized operations of the filter wheel, we have indigenously developed a filter wheel controller card using an A4988 stepper motor driver, Arduino Uno board, and its automated Labview based software to control the rotation of the filter wheel. Since the same controller card and automated software can be used to operate an entirely different filter wheel assembly, it will be possible to use the same in different instruments planned in the future (Ctibor and Pazdera, 2017).

To control the overall system which consists of a stepper motor, stepper driver, and Hall effect sensor we have used Arduino Uno board (Badamasi, 2014) as a master controlling unit. For making the system reliable and robust we have used the feedback of the Hall effect sensor so that the whole system can act as a closed-loop system which helps us, in achieving the precise positioning of filters. Figure 6 shows the schematic circuit for the filter wheel controller in which Arduino interfaces with a stepper driver and Hall effect sensor. Figure 7 shows the PCB design and component mounted PCB of the Filter wheel controller.

It is required that software be developed for getting the filter positions, synchronize their rotation with the CCD imaging, and automate data acquisition. Hence, we have developed Labview based software for filter wheel and CCD module named as filter wheel and camera controller for CMAP. Figure 8 shows the flowchart of the logic implemented in the development of this software for filter wheel and camera controller for CMAP. The software is designed to begin with reading the schedule files that is required to set the various CCD parameters, such as, exposure time, CCD binning, and CCD detector temperature. Once the CCD is tuned to the desired settings which is kept same for all the filters, the filter wheel is rotated and the exposure time for each filter is taken from the profile file which can be different for different filters. Once data is acquired for a particular filter, it rotates again to acquire the data for the next filter, for the duration of exposure time set for it. This process continues for the observational duration of that night as defined in the schedule file. At the end of the data acquisition for a given night the program is designed to wait until the begin time of the next exposure. In this way the data acquisition can be continue in a programmed and automated mode for night after night for several months and years. As the data acquired can be monitored remotely, in case
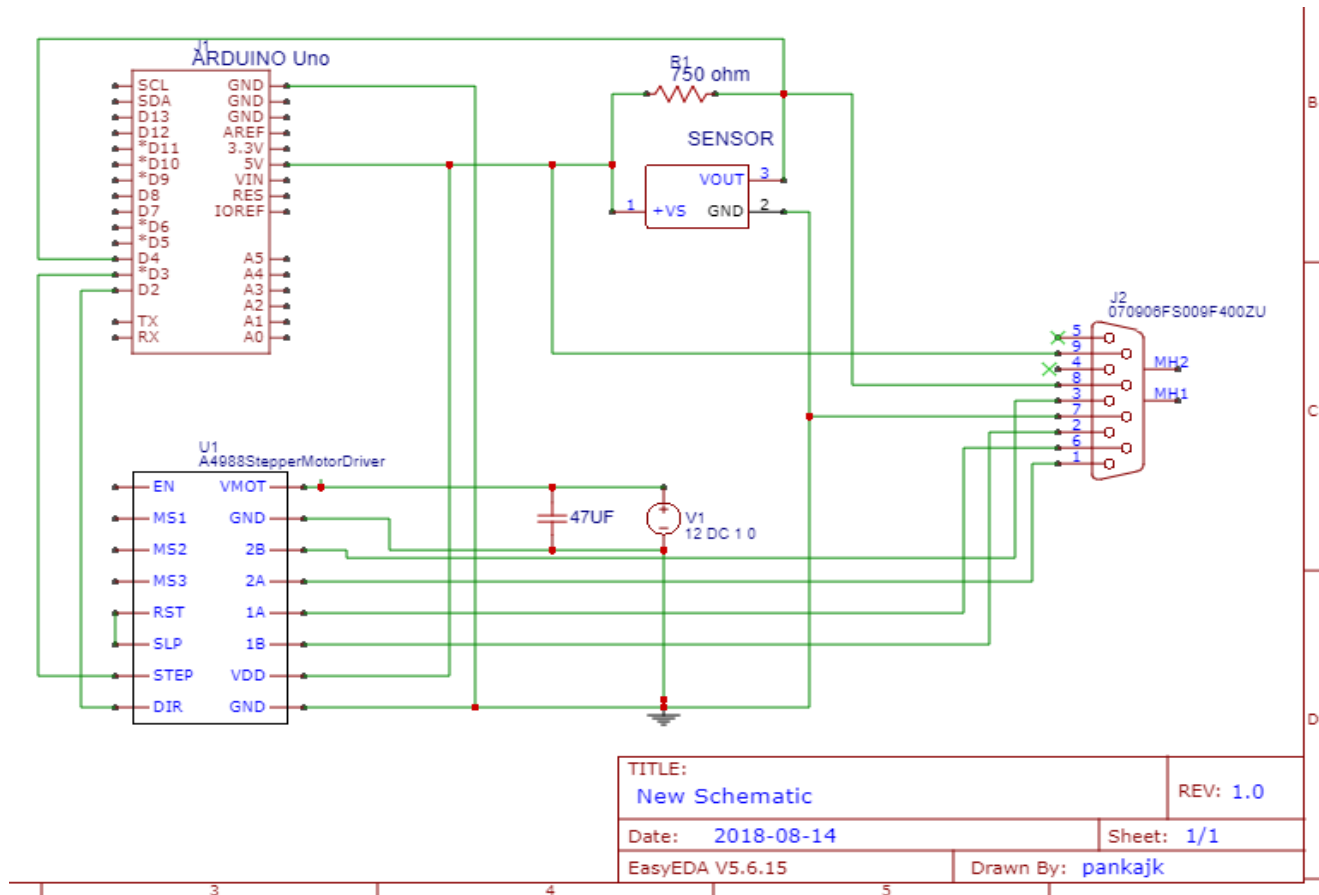
Figure 6. Schematic of filter wheel controller shows the interface between Arduino, A4988 stepper driver, Hall effect sensor (OH180U).
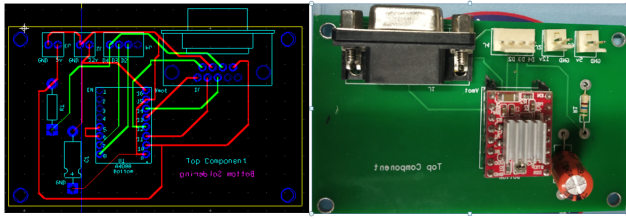
Figure 7. PCB design and components mounted PCB of filter wheel controller.

of any requirement or malfunction, manual intervention can take place.

The three screenshots of the GUI that has been developed for filter wheel and camera controller for CMAP is shown in Figures 9 (a), (b) and (c), respectively. Each screenshot shows different parameter and settings available in the GUI of filter wheel and camera controller. Figure 9a shows the schedule file path settings and filter wheel controls. A full frame image (1024×1024) can be seen on the right side of Figure 9a obtained for a particular filter. Figure 9b shows the filter wheel settings and path in which the images are saved, the different parameters as given in profile file are also displayed, and step settings of filter1. Figure 9c shows the step settings for the rest of four different filters. Figure A1 and Figure A2 shows the part of back-end block diagram of developed CCD imaging and filter wheel control logic.

2.3 Bipolar Temperature Controller

The NBIF filters used in CMAP have operating temperature at 23^oC. Their temperature has to be maintained for a typical operation of around 10 hours to prevent any shift in the wavelength of peak transmission. The transmission spectrum shift slightly to longer wavelength with the increase in temperature. The temperature dependence of an interference filter is given by the equation 1 where λ and λ_o are the shifted and central wavelengths.

$$\lambda(^{\circ}C) = \lambda_o + \Delta T(\Delta\lambda_o/1^{\circ}C) \tag{1}$$

Figure 10 shows a representative plot to illustrate the wavelength shift in a NBIF with reference to temperature for a certain coefficient of temperature. The $\Delta\lambda$ per ^oC is dependent on the gap sensitivity of multi layer coatings in the interference filter. For the interference filters that are used in CMAP, $\Delta\lambda_o$ have typical range of 0.020 nm - 0.025 nm for 1^oC change in temperature. A typical 20^oC change in the ambient temperature leads to a corresponding 0.5 nm shift in the wavelength (equation 1). Since the NBIFs used in CMAP have a typical bandwidth of 0.3 nm, this shift in the wavelength is significant, and hence temperature control of filter wheel chamber is necessary. The bipolar temperature controller can maintain the filter chamber temperature within $\pm0.5^oC$ in the given temperature range. The bipolar temperature control achieved within $\pm0.5^oC$ is well within the limits of shifts in peak transmission wavelengths.
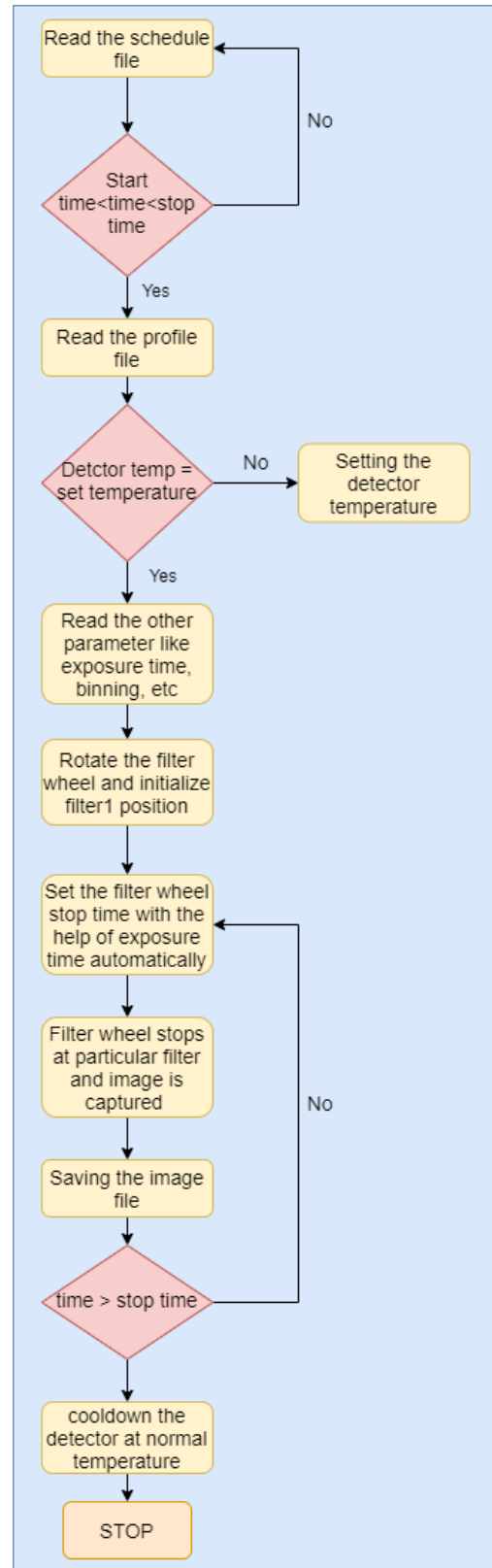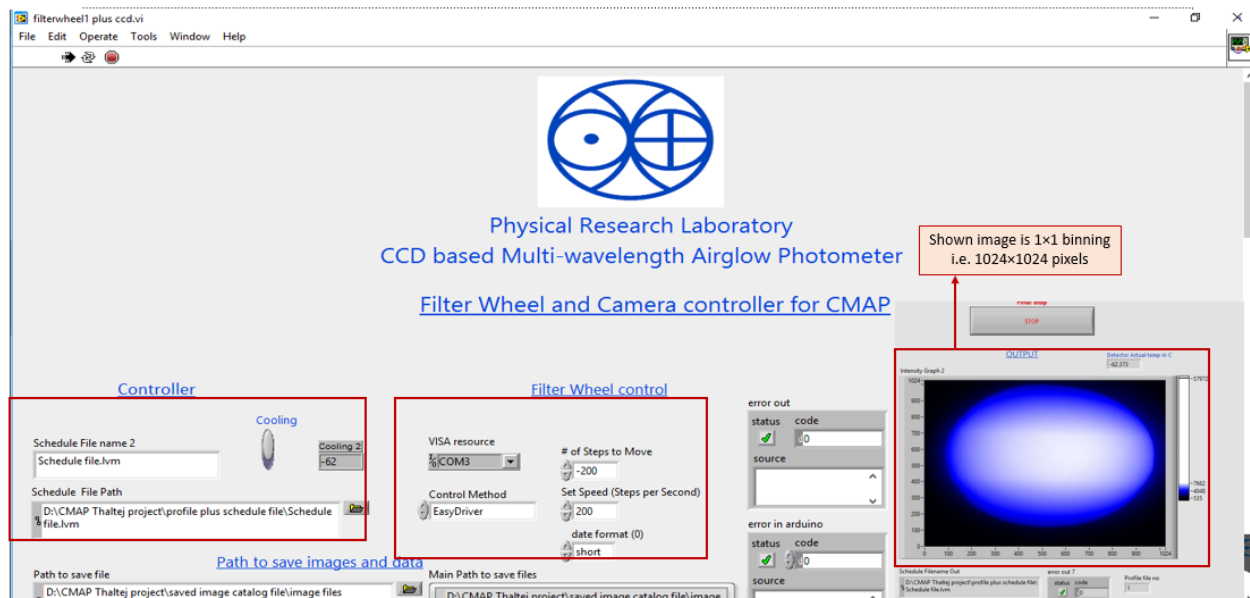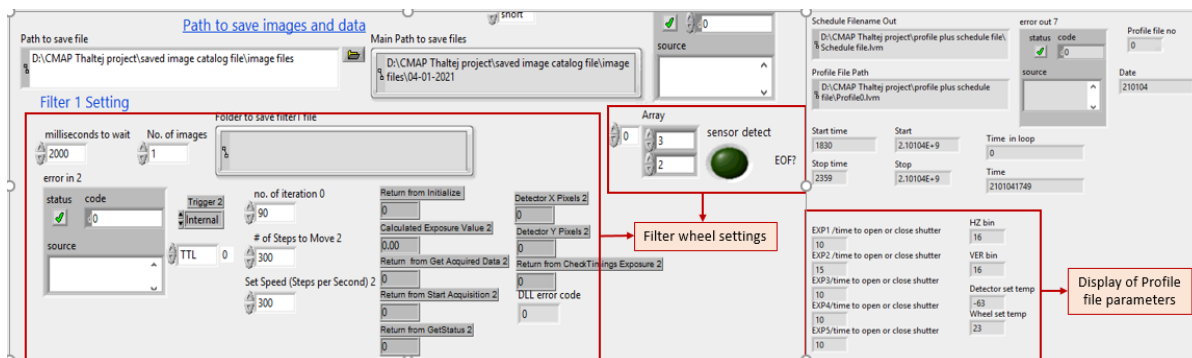

Figure 8. Flowchart of filter wheel and camera controller for CMAP.
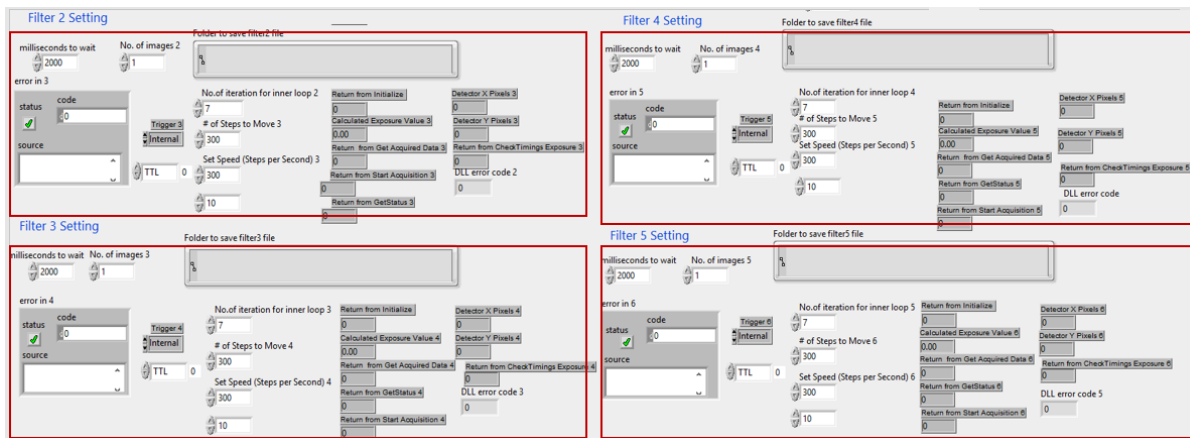
Figure 9. GUI of filter wheel and camera controller for CMAP shows the different parameters and settings available in GUI

(a) Screenshot of filter wheel and camera controller for CMAP GUI shows the different settings for CCD and filter wheel. A full frame image of 1024×1024 pixel is shown in the right side of the figure.

(b) Screenshot of filter wheel and camera controller for CMAP GUI shows the different settings for filter wheel, path to save, image and catalog files. It also displays the parameter of profile file for the purpose of monitoring.

(c) Screenshot of filter wheel and camera controller for CMAP GUI shows the different settings for filter wheel, path to save, image and catalog files for the rest of four different filters.
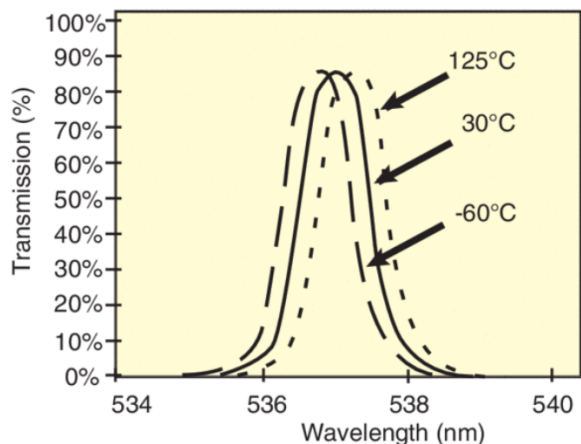
Figure 10. Representation of Wavelength shift in optical filter with temperature. (Courtesy- https://www.newport.com/n/stabilife-coating)
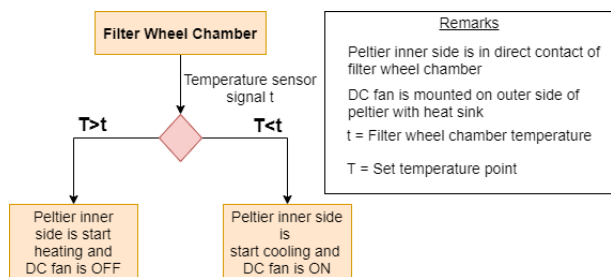

Figure 11. Logical operation of DC fan with Peltier element.

Presently, the filter chamber consists of 5 filters with a diameter 50 mm each and the overall dimension of 196 mm x 185 mm x 30 mm. For the development of bipolar temperature controller, we have used military grade Peltier components as a thermoelectric element with heat sink and DC fans, L298 motor drivers for changing the polarity of the Peltier element. For temperature measurement we have used analog thermal sensors, OpAmp based amplifier for amplification of analog signal, Arduino Uno board as a microcontroller and heat sink compound for mounting the Peltier elements.

2.3.1 Peltier Element

The Peltier effect is a reverse phenomenon of the Seebeck effect in which a potential difference between the two junctions generates the temperature gradient between the junctions. In a Peltier element, voltage is applied across the conductors to create an electric current. When the current flows through the junctions of the two conductors, heat is removed at one junction and cooling occurs (cold junction) and this heat is deposited at the other junction (hot junction). In this way one side of the Peltier element provides cooling and other side provides heating. By reversing the polarity of voltage supplied, the current flows in a reverse direction and the hot and cold junctions are reversed. The simplified operation of a fan and a Peltier element is shown in Figure 11.

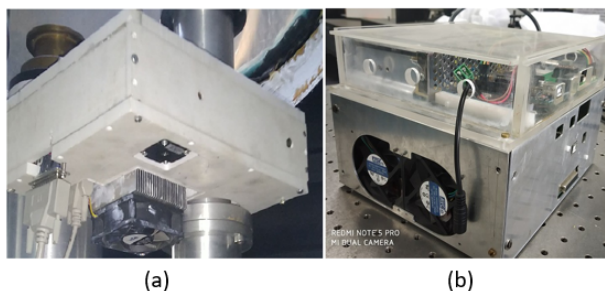Taking into consideration the important features of Peltier

Figure 12. Photograph (a) filter wheel chamber showing DC fans and teflon case, (b) electronic box of CMAP in which all the controller cards and power supply are mounted.

elements, like reliability for high thermal cycling, superior thermal performance, wide ΔT_{max} of almost $60^o C$ at room temperature and precise temperature control, we have identified the CP85H series of Peltier elements to be the most suitable ones for our application. The characteristics of this series of Peltier elements are shown in Table 1.

The CP854345H Peltier element can maintain the ΔT_{max} of $70^o C$ at $27^o C$ room temperature as mentioned in Table 1 when its surface is in direct contact with the Peltier element. However, the overall dimension of filter chamber is 196 mm x 185 mm x 30 mm is quite large in our case. Hence, in order to control the temperature of filter chamber within the accuracy of $\pm 0.5^o C$ we have chosen eight elements of CP854345H Peltiers whose input voltage is 15.7 Volt (max) and current rating is 8.5 Ampere (max) in which four Peltier elements are placed on the bottom plate of the filter chamber and the other four are placed on the top of the filter chamber. We have used two analog temperature sensors and placed them at two independent and physically opposite locations of the filter chamber so as to obtain a fair assessment of the chamber temperature. The average temperature from both these sensors is taken as the resultant temperature of the filter chamber. The whole filter chamber is placed in a Teflon case to insulate the filter chamber temperature from that of the ambient environment.

Figure 12 shows the overall structure of the filter chamber with DC fans. It also shows the electronic box of CMAP instrument in which the temperature controller card, filter wheel controller, and power supply are assembled. Subsystem like CCD requires an ambient of $27^o C$ for the desired cooling of the detector. Hence, we have tested the filter chamber at ambient temperatures in the range of $18^o C$ to $30^o C$ for the set temperature of $23^o C$.

2.3.2 Electronics of Bipolar Temperature Controller

Bipolar temperature controller operational block diagram is shown in Figure 13 in which the following are important components:

- Bipolar Driver (L298N): To make temperature controller bipolar, we need to use a suitable driver through which we can change the polarity of the Peltier elements. These drivers are based on the H-bridge principle as shown in

MODEL	input voltage[1] max (Vdc)	input current[2] max (A)	internal resistance[3] typ ($\Omega\pm10\%$)	output Qmax[4]		output ΔTmax[5]	
				$T_h=27°C$ (W)	$T_h=50°C$ (W)	$T_h=27°C$ (°C)	$T_h=50°C$ (°C)
CP85134H	2.1	8.5	0.2	10.3	11.3	70	77
CP85153034H	4.2	8.5	0.4[7]	21	23	70	77
CP85234H	3.8	8.5	0.35	18.8	20.8	70	77
CP852040345H[6]	7.6	8.5	0.75	38.2	42	70	77
CP85301534H	4.2	8.5	0.4[7]	21	23	70	77
CP853345H[6]	8.8	8.5	0.85	43.1	48	70	77
CP8530345[6]	11.8	8.5	1.15	57.7	63.4	70	77
CP854020345H[6]	7.6	8.5	0.75	38.2	42	70	77
CP854345H[6]	15.7	8.5	1.5	77.1	85	70	77

Notes:
1. Maximum voltage at ΔT max and T_h=27°C
2. Maximum current to achieve ΔT max
3. Measured by AC 4-terminal method at 25°C
4. Maximum heat absorbed at cold side occurs at I_{max}, V_{max}, and ΔT=0°C
5. Maximum temperature difference occurs at I_{max}, V_{max}, and Q=0W (ΔT max measured in a vacuum at 1.3 Pa)
6. Designed with arcTEC™ structure.
7. Internal resistance tolerance is ±12.5%

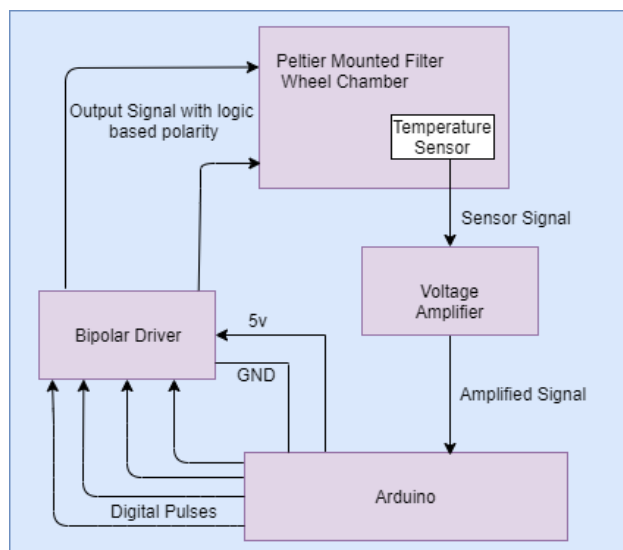**Table 1.** Characteristics of CP85H Peltier series.
(Courtesy-`https://www.cuidevices.com/product/resource/cp85.pdf`)

Figure 13. Electronics block diagram of temperature controller.
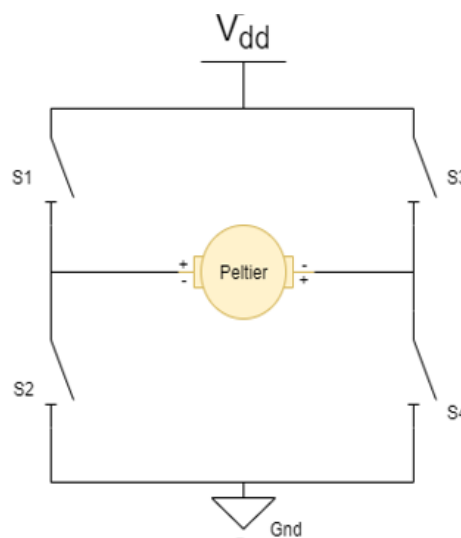

Figure 14. H-Bridge logic diagram showing the principle for change of polarity for Peltier element.

Figure 14. Here, we have used commercially available bipolar motor driver L298N, which is controlled by an Arduino Uno board. The major advantage of L298N is that it can draw a current up to 2 Amperes. Hence, the rates of cooling and heating are increased in a significant manner.

• Temperature Sensor (LM35): We have used analog temperature sensors but due to weak output signal of the sensor we have also applied the voltage amplifier to boost the voltage signal and then its output is fed into the A/D pin of arduino in order to read the temperature of the chamber continuously.

- Arduino Board: Arduino is used for generating the logic based digital signal for heating and cooling operations. We have used the inbuilt A/D converter of Arduino to convert the sensor analog voltage into digital voltage. Further, Arduino is used to communicate between Labview based software and electronics hardware with the help of a Labview module named Labview Interface for Arduino (LIFA). The schematic diagram of temperature controller is shown in Figure 15 in which Arduino is interfaced with L298N drivers and temperature sensors. The PCB design and component mounted PCB board of temperature controller is shown in Figure 16.

2.3.3 Software Development of Bipolar Temperature Controller

Fully automated Labview based software is developed for bipolar temperature controller. In the software, the temperature feedback value is obtained by averaging the temperature data for the 30 sample points (with the sampling of 1 sec) which is fed to the designed logic to stabilize the temperature over time. Therefore, instead of providing proportional current, we are carrying out pulse width modulation (PWM) (Barr, 2001) with variable duty cycle (depends on the difference between the set and actual temperature) using L298N driver, which effectively is proportional to the difference between the set and actual temperature. The whole hardware and software of temperature controller are designed in such a way that they can be used in other instruments whenever chamber temperature is needed to be controlled.

Figure 17 shows the flow of bipolar temperature controller program, which shows that after reading the schedule file temperature is stabilized with the help of L298N bipolar drivers. Figure 18 shows a screenshot of GUI of the bipolar temperature controller in which we can set the chamber temperature either manually or through the input file (profile file). Figure 18 shows the profile file parameters like exposure time, binning, detector temperature, and filter wheel temperature. Figure A3 shows the back-end block diagram of bipolar temperature controller for CMAP.

For the normal operation of CMAP, first we have to run bipolar temperature controller GUI which stabilizes the temperatures of NBIF filters, and then filter wheel and camera controller for CMAP GUI which sets the filter wheel and CCD parameters.

3. CMAP Software Development and its Automation

We have described the development of CCD imaging software, filter wheel, and bipolar temperature controller units in terms of hardware and software design perspectives. To operate the CMAP, these units have to be integrated, synchronized, and controlled as per the requirement. We have used two Arduino Uno boards, one is used in the filter wheel and the other is used in the bipolar temperature controller as a microcontroller. LIFA module is used in Labview for Arduino

clock and I/O instructions. To achieve proper synchronization between the subsystems and differentiate the I/O instructions, we have created two executable (.exe) programs. (i) "Filter wheel and Camera controller for CMAP" to control the CCD and filter wheel, and (ii) "Bipolar Temperature controller" to control the filter chamber temperature. Both the .exe programs need to run simultaneously for the operation of CMAP.

The two text files are generated wherein all the parameters can be defined. These parameters are: filter chamber temperature exposure time for each of the filters, CCD detector temperature, the dates, begin and end time of the operation, etc. These two files acts as an input file to run both GUI's as mentioned earlier.

1. Profile File: This file consists of image exposure time for all the filters, Horizontal and Vertical binning of the image, set temperature for the CCD detector, and set temperature for the filter wheel chamber. The Figure 19 shows the format of a profile file in which arguments are separated by commas. This provides flexibility to create many profile files named as profile0, profile1, profile2, etc., with different parameter values as per the experimental conditions and it can be modified by the user at any time.

Figure 19. Sample of Profile File.

2. Schedule File: This file is used for the scheduling of the experiment. It consists of Date (in YYMMDD format), Start Time (in HHMMSS format), Stop Time (in HHMMSS format) and Profile File. Each line of the file accepts one schedule i.e start and stop time of the experiment. There can be many schedules in a single scheduled file for e.g. we can have the schedule of a whole year in a single schedule file or multiple schedules to be followed even in a given night. The Figure 20 shows the format of schedule file in which arguments are separated by commas.
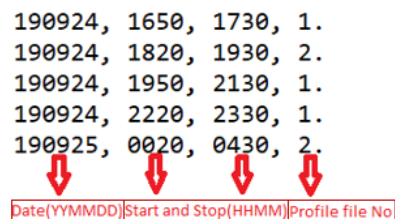

Figure 20. Sample of schedule file.

Figure 15. Schematic of temperature controller shows the interfacing between Arduino, bipolar driver (L298N), and temperature sensor (LM35).
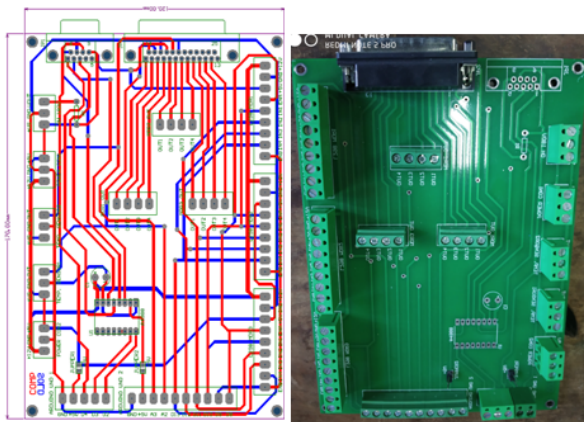
Figure 16. PCB design and PCB board of temperature controller.

Generation of .exe file: In order to use this program at multiple locations it is required that the software be not tied to the presence of Labview software in the computer mandatorily, as it is expensive, and therefore, it is not optimal that it is compulsorily required to be present on the computer which is used to run the CMAP. Hence, for making our project cost efficient and the software to be portable on any commercial PC, we have created an executable file (.exe file) which can be run on any PC with just the presence of Labview Runtime engine installed in it (Stratoudakis, 2009). The labview runtime engine is available on the NI website and is free of cost.

In order to run CMAP and record data at pre-defined settings, the following steps are followed.

1. We have to connect the CCD, filter wheel, and temperature controller using USB connectors.

2. Two USB connector needs to connect with com port of the PC. 25 pin and 9 pin D-connector are directly connected with D-connectors of electronic box.

3. In any PC with Windows 7 or above, minimum 4GB RAM is required to operate the CMAP software. Install the Labview runtime engine and andor CCD software on the PC.

4. Put the .exe file of CMAP imaging and bipolar temperature controller software which consists of both the the GUI in the startup of windows in order to run the program automatically when the PC is turned on.

5. Create the path for reading the schedule and profile file. Create the path for storing the image, filter temperature and catalog file as mentioned in both the GUI.

We have developed an integrated software of CMAP in Labview in which the image acquisition is done through the following steps:

1. Run the schedule file in the software in a continuous manner and continually scan for the start date and time
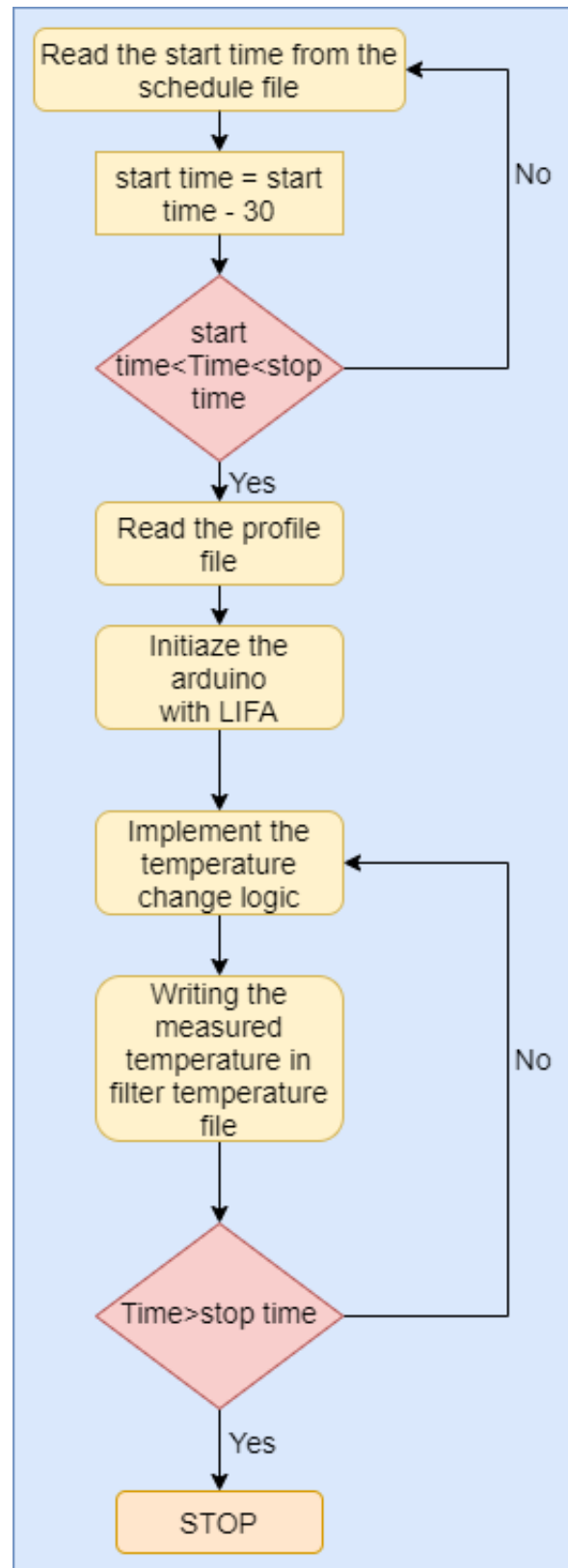

Figure 17. Flowchart of bipolar temperature controller showing the flow of back-end logic.
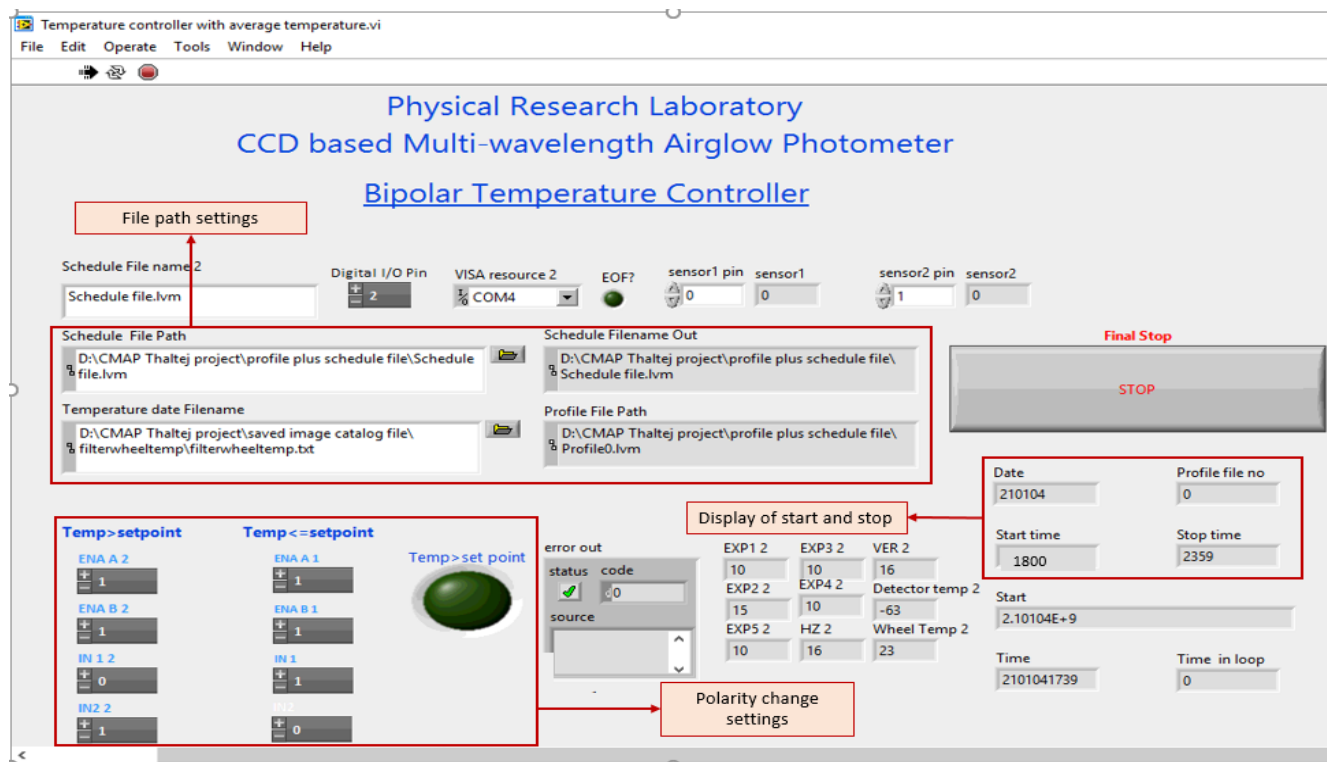
Figure 18. Screenshot of the GUI used for bipolar temperature controller which shows the settings for file path and change of polarity.

and compare with the computer time to initiate or wait to perform the experiment.

2. Once the schedule is matched, detector temperature and filter wheel the temperature will set to the desired temperature value as indicated in the profile file.

3. The profile file also consists of information on the binning, exposure time and number of images per filter required for the experiment. This profile file is read and the parameters as indicated in the profile file are set in the program.

4. With the help of Hall effect sensor feedback program reinitialize the filter position.

5. The wheel rotates and stops for that particular exposure time (as set in the profile file), image will be taken by the CCD and then it saves it in flexible image transport system (.fits) format in the predefined folder for the output files.

6. The task mentioned in point 5 repeats continuously until the stop time set in the schedule file is reached.

7. During the whole operation, the temperature controller is running continuously in order to maintain the filter chamber's temperature at the defined set value.

Figure A4 shows the part of back-end block diagram for the scheduling logic creation of CMAP software. Figure 21 shows

the photograph of CMAP mounted in Optical Aeronomy observatory at PRL's Thaltej campus for field operations. CMAP is mounted in a vertical direction and the optical dome at the top of CMAP can be seen in Figure 21.

4. Data Acquisition and Analysis

A typical image obtained by CMAP is shown in Figure 22. The final CMAP data consists of images in FITS format with the relevant parameters like exposure time, binning, detector temperature, date, and time of the image which are stored in a separate text file named as catalog file. A sample of catalog file showing various desired parameters of the instrument is shown in Figure 23. The catalog file records the exposure time, binning, CCD temperature in their respective folders for each filter with date, year and frame name which contains station name, hh, mm, ss, and day of year (e.g., amd010849.111.fits).

We also need to monitor the continuous temperature of filter wheel chamber. Therefore, the temperature of the filter wheel chamber is stored by the GUI of bipolar temperature controller which creates a separate file for each day. This file contains the actual chamber temperature, set temperature, date, and time as shown in Figure 24. For acquiring the data from "filter wheel and camera controller for CMAP GUI", we have created the respective folders for different wavelengths. The data folders consist of image files and catalog files in which images are saved in .fits format. Filter wheel temperature files are saved in the different folders that are automatically created and named as per the date of observation.
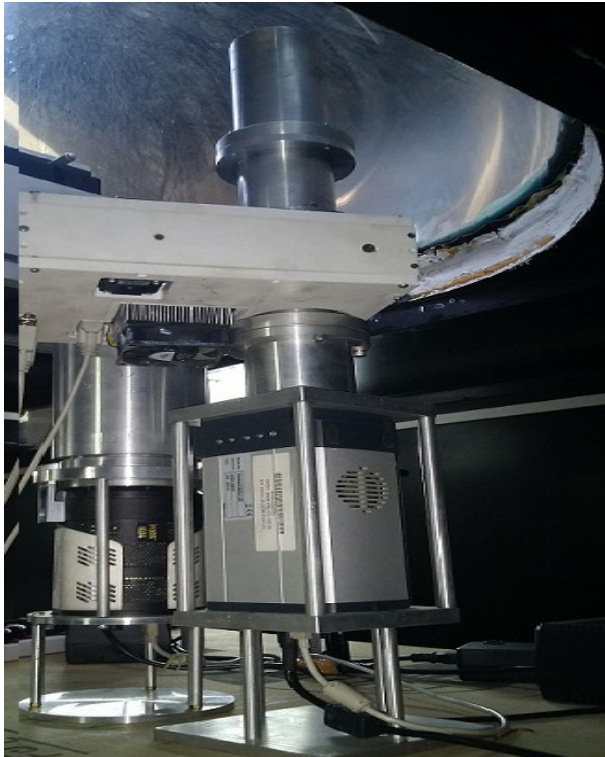
Figure 21. Photograph of CMAP operating from the Optical Aeronomy observatory at PRL's Thaltej campus. The filter wheel assembly and the optical dome on the top can be seen clearly.
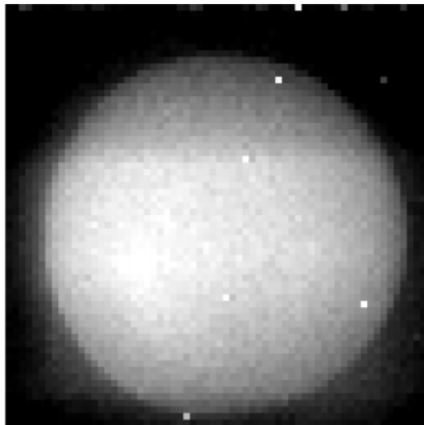

Figure 22. A sample of fits image showing the exposed area of CCD detector which is used to calculate the airglow emission brightness.

There are mainly four parameters that contributes to errors in the pixel counts of the recorded raw images i.e. filter temperature, light leakage, stray light, and CCD dark count. The contribution of unwanted sources needs to be taken into account for making the correct estimates of airglow brightness otherwise it may lead to the error in the estimation of airglow brightness. Before analyzing the CMAP data we need to make sure that the filter temperature remains within the tolerance limit of $\pm 0.5^o C$. In order to stabilize the temperature of filter
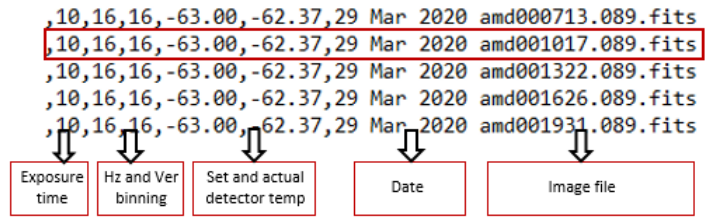

Figure 23. Catalog file data format showing CCD parameters for each of the fits images.
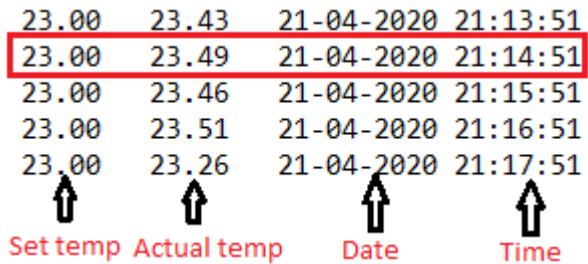

Figure 24. Filter wheel temperature file showing the set and actual temperature generated by bipolar temperature controller GUI.

chamber, it is required that the bipolar temperature controller is turned on 30 minutes prior to the operation of filter wheel and camera controller.

To show the obtained temperature stability of the filter wheel chamber temperature a plot between filter temperature and time is shown in Figure 25. The blue color crosses show all the temperature values for the month of March 2020. This shows the filter wheel chamber temperature remains within the tolerance limit of $\pm 0.5^o C$ for a given month. The green color line shows the nocturnal variations in temperature for the night of 29 March 2020. It can be seen that the temperature values remain within $\pm 0.5^o C$ for the given night.

Data analysis Algorithm: At present the exposure times for the filters 557.7 nm, 630.0 nm, 840.0 nm, 846.6 nm and 857.0 nm are 10, 15, 10, 10, 10 seconds, respectively. Therefore, the data cadence for each filter turns out to be around 1 minutes which is sufficient as the atmospheric oscillations
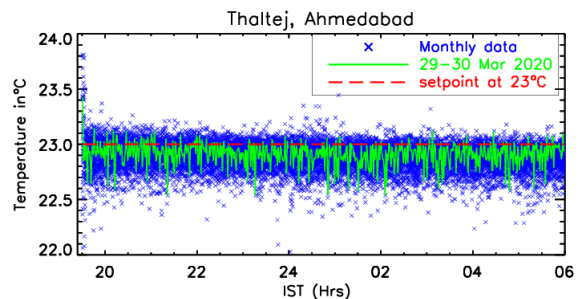

Figure 25. Temperature stability curve for filter wheel chamber with set temperature at $23^o C$ for 30 days of data obtained from Thaltej, Ahmedabad in blue color. The highlighted plot shown in green color is for the night of 29 March 2020 obtained from Thaltej, Ahmedabad.
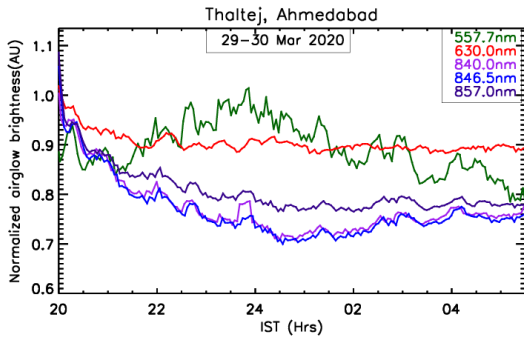
Figure 26. Nocturnal variation of airglow emission brightness at multiple wavelengths obtained for the night of 29 March 2020 from Thaltej, Ahmedabad. As mentioned in the text, it has five filter named as filter1, filter2, filter3, filter4 and filter5 of central wavelength at λ_1 = 557.7 nm, λ_2 = 630.0 nm, λ_3 = 840.0 nm, λ_4 = 846.6 nm and λ_5 = 857.0 nm respectively and have bandwidths in the range of 0.3 nm to 0.5 nm.

(Brunt Vaisala periods) mesospheric and thermospheric altitudes vary from 5-12 minutes. The data analysis procedure is written using IDL software. To increase the SNR of the instrument a 16×16 binning has been used in CMAP, therefore each image will have the size of 64×64 pixels. The CCD temperature has been set at -63°C which reduces the dark counts significantly.

The hot pixels as shown in Figure 22 are mainly due to the incident cosmic rays that are removed using the sigma filter. The sigma filter replaces pixel values with counts more than a specified value from its neighbouring pixels. The information of the dark current is obtained by taking unexposed areas (corners) of the raw images as shown in Figure 22. This dark count value is subtracted from the raw image to obtain the dark subtracted image. The airglow brightness is estimated by choosing the centroid circular area of the image (as shown in Figure 22).

The airglow brightness is obtained for each of the emission lines. Figure 26 represents the nocturnal variations of all the five airglow emissions that emanate from different altitudes of MLT region for the night of 29 March 2020. The time series obtained as shown in Figure 26 is used for further analysis to understand various coupling and dynamical processes in the upper atmospheric region from where the given emission emanates.

5. Future Plans

The plan is to replicate several units of CMAP to enable their deployment at multiple locations of scientific interest for a comprehensive investigations of upper atmospheric phenomenon. In addition, we are in the process of indigenous development of the mechanical structure of filter wheel. The present software is compatible with Andor CCD. Based on the experience gained on the development of the present CMAP we can plan to develop an entirely new instrument which will be compatible with other commercially available CCDs like Princeton, Atik, etc.

References

https://andor.oxinst.com/products/ixon-emccd-cameras.

https://www.pololu.com/product/1182.

https://datasheetspdf.com/pdf/1430672/TT/OH180U/1.

https://www.spectralproducts.com/FilterWheels.

https://www.newport.com/n/stabilife-coating.

https://www.cuidevices.com/product/resource/cp85.pdf.

Y. A. Badamasi. The working principle of an arduino. In *2014 11th international conference on electronics, computer and computation (ICECCO)*, pages 1–4. IEEE, 2014.

M. Barr. Pulse width modulation. *Embedded Systems Programming*, 14(10):103–104, 2001.

D. Chakrabarty. Investigations on the f regions of the ionosphere over low latitudes using optical, radio and simulation techniques. *Ph.D. Thesis*, 2007.

J. Ctibor and I. Pazdera. The new stepper driver for low-cost arduino based 3d printer with dynamic stepper control. In *International Conference Mechatronics*, pages 458–466. Springer, 2017.

F. I. Laskar, D. Pallamraju, T. V. Lakshmi, M. A. Reddy, B. Pathan, and S. Chakrabarti. Investigations on vertical coupling of atmospheric regions using combined multiwavelength optical dayglow, magnetic, and radio measurements. *Journal of Geophysical Research: Space Physics*, 118(7): 4618–4627, 2013.

R. Narayanan, J. Desai, N. Modi, R. Raghavarao, and R. Sridharan. Dayglow photometry: a new approach. *Applied Optics*, 28(11):2138–2142, 1989.

D. Pallamraju, R. Sridharan, S. Gurubaran, and R. Raghavarao. First results from ground-based daytime optical investigation of the development of the equatorial ionization anomaly. In *Annales Geophysicae*, volume 14, page 238, 1996.

D. Pallamraju, F. I. Laskar, R. P. Singh, J. Baumgardner, and S. Chakrabarti. MISE: A multiwavelength imaging spectrograph using echelle grating for daytime optical aeronomy investigations. *Journal of Atmospheric and Solar-Terrestrial Physics*, 103:176–183, 2013.

K. A. Phadke, R. P. Narayanan, Singh, and D. Pallamraju. An automated ccd-based multi-wavelength airglow photometer (cmap) for optical aeronomy studies. *PRL-TN-2014-107*, 2014.

S. Sarkhel. Upper atmospheric investigations using radio and optical techniques. *Ph.D. Thesis*, 2010.

R. P. Singh. Investigations of interactions in the earth's upper atmosphere using optical and radio wave techniques. *Ph.D. Thesis*, 2017.

R. P. Singh and D. Pallamraju. Effect of cyclone nilofar on mesospheric wave dynamics as inferred from optical nightglow observations from mount abu, india. *Journal of Geophysical Research: Space Physics*, 121(6):5856–5867, 2016.

R. P. Singh and D. Pallamraju. Near infrared imaging spectrograph (NIRIS) for ground-based mesospheric OH(6-2) and O2 intensity and temperature measurements. *Journal of Earth System Science*, 126(88):1–17, 2017.

R. Sridharan, N. Modi, D. P. Raju, R. Narayanan, T. K. Pant, A. Taori, and D. Chakrabarty. A multiwavelength daytime photometer-a new tool for the investigation of atmospheric processes. *Measurement Science and Technology*, 9(4):585, 1998.

T. Stratoudakis. Building applications with labview. Technical report, ALE System IntegrationMelville, New York, 2009.

7. Appendix A

Figure A1 is a part of back-end block diagram of CCD imaging program. It shows the different logic creation of catalog file data generation, creation of catalog filename format, writing of measurement file by using the different modules available in Labview.
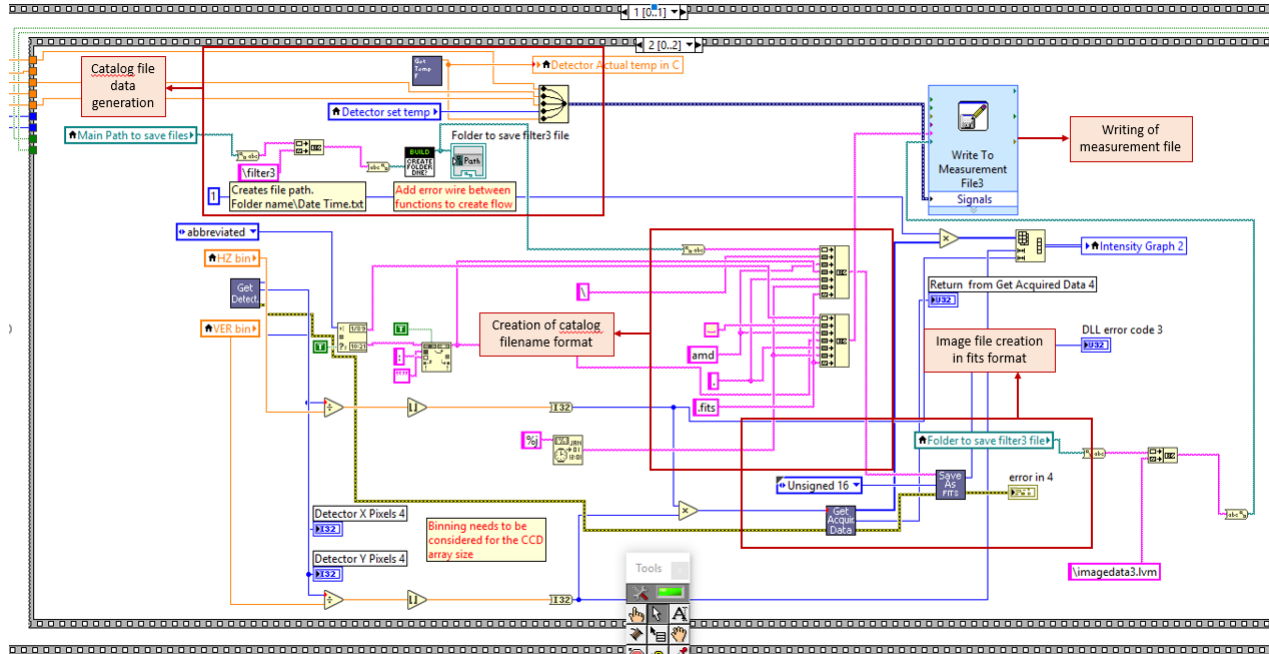

Figure A1. Back-end block diagram showing the logic used for implementing various CCD parameters and data acquisition for CMAP software.

Figure A2 is a part of back-end block diagram of the CCD imaging program. It shows the different logic creation for filter wheel rotation like Arduino initialization and digital pin setting, hall sensor detection, stepper steps settings, and steps setting for each filter by using the different modules available in Labview.
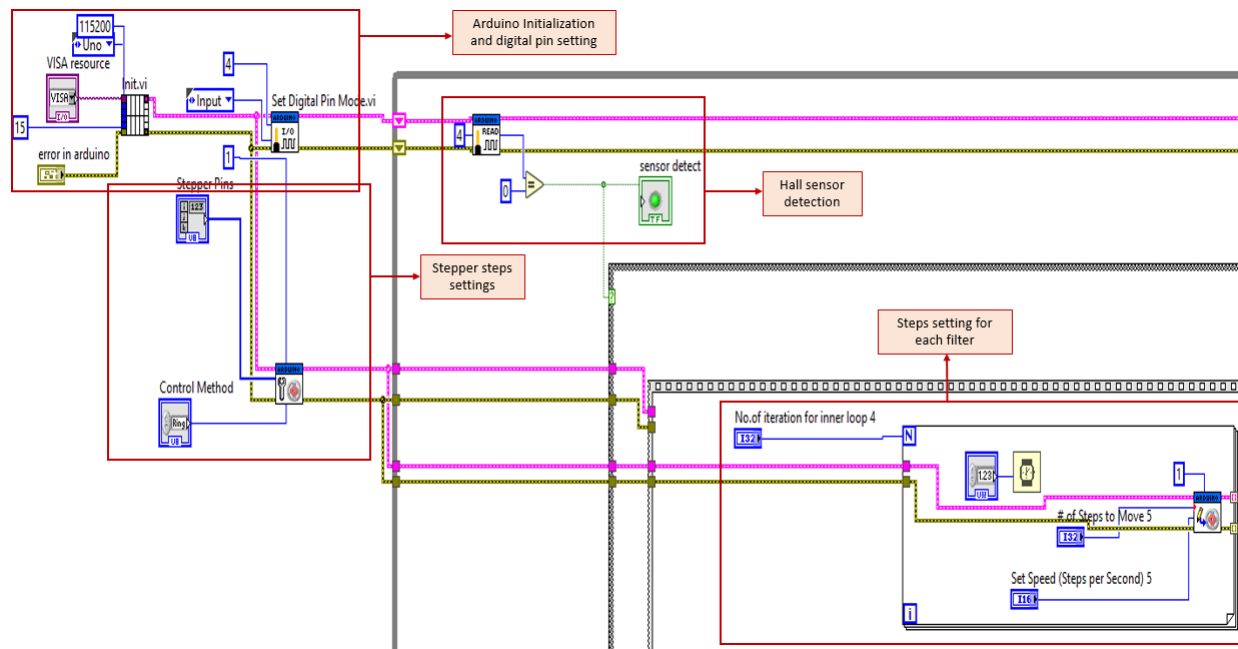

Figure A2. Back-end block diagram for the logic creation of stepper steps for filter wheel control.

Figure A3 is a part of a back-end block diagram of bipolar temperature controller program. It shows the different logic creation for temperature control like Arduino initialization and digital pin setting, temperature reading from Arduino analog pin, creation of boolean case for polarity change and writing the chamber temperature in the predefined format by using the different modules available in Labview.
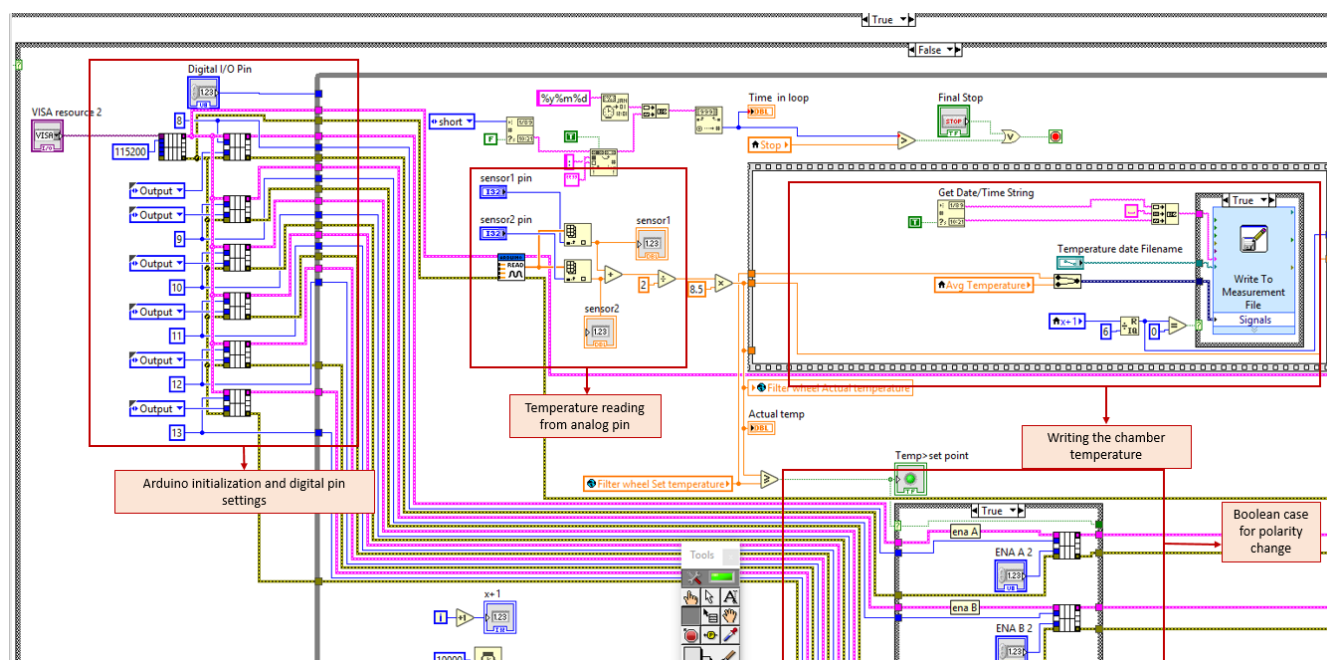

Figure A3. Back-end block diagram of bipolar temperature controller shows the polarity change and temperature data acquisition logic

Figure A4 is a part of a back-end block diagram of the CMAP software program. It shows the different logic creation for reading the schedule file, display of parameters of schedule file and profile file, and logic creation for scheduling operation of CMAP by using the different modules available in Labview.
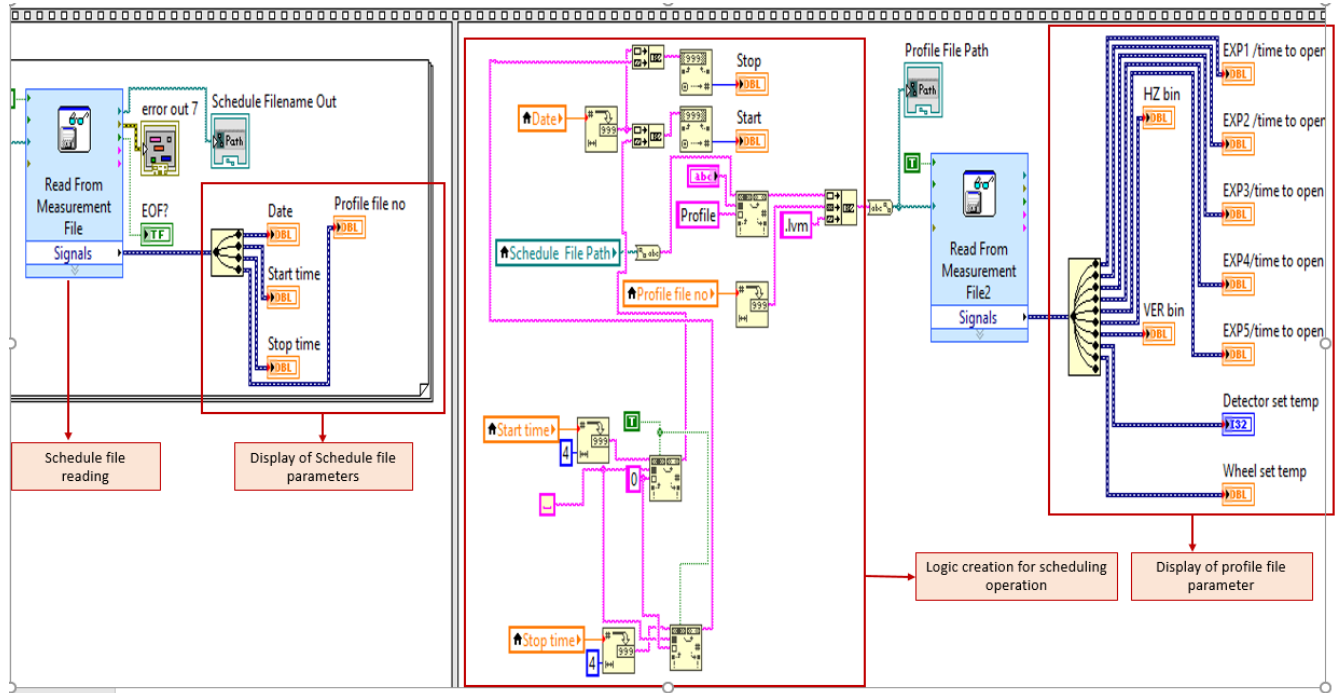

Figure A4. Part of back-end block diagram of CMAP software shows the scheduling and profile file reading logic

PRL research
encompasses
the earth
the sun
immersed in the fields
and radiations
reaching from and to
infinity,
all that man's curiosity
and intellect can reveal

पीआरएल के
अनुसंधान क्षेत्र में
समविष्ट हैं
पृथ्वी एवं
सूर्य
जो निमीलित हैं
चुंबकीय क्षेत्र एवं विकिरण में
अनंत से अनंत तक
जिन्हे प्रकट कर सकती है
मानव की जिज्ञासा एवं विचारशक्ति